NASA Technical Memorandum 81572

WIND TUNNEL INVESTIGATION OF THE TITAN FORWARD SKIRT COMPARTMENT VENT FROM A FREE-STREAM MACH NUMBER OF 0.80 TO 1.96

Albert L. Johns
Lewis Research Center
Cleveland, Ohio

September 1980

NASA

WIND TUNNEL INVESTIGATION OF THE TITAN FORWARD SKIRT COMPARTMENT VENT FROM A FREE-STREAM MACH NUMBER OF 0.80 TO 1.96

by

Albert L. Johns

SUMMARY

An experimental program was conducted in the Lewis Research Center 8-by-6-Foot Supersonic Wind Tuunel to determine the flow characteristics of the Titan Forward Skirt compartment vent. The test was conducted over a free-stream Mach number range of 0.80 to 1.96 with the vent mounted in a flat plate. The plate was flush mounted to the tunnel sidewall with coinciding center lines. Air was discharged from a duct, located on the tunnel sidewall behind the plate, through a honeycomb vent into the free-stream. The test was conducted to provide data for the analysis of the Titan Forward skirt compartment venting during ascent through the atmosphere. Full scale simulated flight hardware, such as the honeycomb vent, duct, ("super-zip" strip) explosive separation strip, corrugations and field joint ring were used.

Boundary layer thickeners were used to vary the boundary layer height and profiles. The thickeners consisted of several rods which were fastened to a plate mounted at the leading edge of the test section. The boundary layer height varied from a maximum of 26.00cm at Mo= 0.90 to a minimum of 16.51cm at Mo= 1.40.

The highest vent discharge coefficient for any given Mach number and vent pressure ratio generally occurred at the maximum displacement thickness. With no vent flow, the static pressures downstream of the field joint ring (includes the vent region) were generally less than free-stream static pressure.

INTRODUCTION

During ascent through the atmosphere, several compartments in the Titan/Centaur launch vehicle are vented overboard into the freestream. The venting during this section of the flight must be controlled in such a way that the compartment walls are not exposed to excessive crush on burst pressures. In utilizing a vent system that will meet this requirement, consideration must be given to the phenomenon that occurs at the vent outlet when the vented gas impinges the air stream moving over the surface of the vehicle. The interaction of the exiting jet with the external flow results in a local external pressure higher than that which would exist without the vent flow, ref. 1. The need to include the geometric environment in the venting characteristics study is obvious, since it will affect the local vent pressure, ref. 2, which is directly related to the vent flow rates. Other work has been done to investigate the effects of the exiting jet-freestream interaction phenomenon, ref's. 3 through 9.

One of the compartments to be vented during atmospheric ascent is the Titan forward skirt compartment which is located aft of the Centaur boattail. This compartment is vented through ducts running forward of the Centaur boattail. The vent configuration consists of honeycomb vents 12.70cm (5 in.) by 7.62cm (3.00 in) located downstream of a field joint ring and upstream of the super-zip region.

This report documents the discharge characteristics of the Titan Forward skirt (6-2) honeycomb vent configuration with various external environmental conditions. A secondary objective was the determination of aerodynamic pressures in the vicinity of the vent.

The test was conducted in the Lewis Research Center 8- by 6-Foot Supersonic Wind Tunnel over a range of Mach numbers from 0.80 to 1.96. The test configuration consisted of a full-scale simulation of the honeycomb vent which was mounted on a flat plate attached to the wind tunnel wall. Also included were a full-scale section of shroud corrugations and other protuberences which are located in the vicinity of the vent. Air was discharged through the honeycomb vent into the wind tunnel freestream from the full-scale simulated duct which was mounted on the backside of the tunnel wall.

SYMBOLS

Cp, CP	pressure coefficient, $(P_l-P_o)/q_o$
K	Vent discharge coefficient based on one-dimensional flow rate which assumes a static pressure obtained from an average pressure upstream (orifice 202) and downstream (orifice 204) of the vent when there is no vent flow.
LREF	Reference length, LREF=2.54cm(1.00 in.)
M_o, MO	free-stream Mach number
M_l, ML	local Mach number based on orifice 202
P_l	Local static pressure
P_o	free-stream static pressure
PE/PI	Vent pressure ratio, ratio of an average pressure upstream (orifice 202) and downstream (orifice 204), no vent flow, to duct pressure
q_o	free-stream dynamic pressure
VL/VLMAX	Boundary-layer velocity ratio (local velocity to local maximum velocity)
X/LREF	axial distance from tunnel station 650.75cm (256.20 in.)-to-reference length where reference length, LREF=2.54cm (1.00 in.)
Y	normal distance from trough of corrugated surface
δ	boundary-layer thickness, height of the boundary layer where local velocity becomes 99 percent of maximum local velocity
δ^*	displacement thickness, a measure of deficiency in mass flow through the boundary-layer as a result of the steam having been slowed by friction
H	Shape factor - ratio of displacement thickness-to-momentum thickness. Where momentum thickness is the thickness of the freestream flow necessary to make up the deficiency in momentum flux within the boundary layer

APPARATUS

The test installation in the wind tunnel is shown in figure 1. The plate was flush mounted to the tunnel sidewall with the centerline of the plate and tunnel wall coinciding. The plate was located 92.70 centimeters (36.50 in.) downstream of the boundary layer thickener plate, figure 1. Sections of full-scale simulated flight hardware such as the honeycomb vent, the shroud corrugations, aft field joint ring, and super-zip were attached to the plate, figure 1(b). The installation of the boundary-layer rakes is shown in figure 1(c).

A schematic of the vent flow system is shown in figure 1(d). The Titan forward skirt duct was attached to the backside of the tunnel sidewall. Air was obtained from the atmosphere. The flow rate was measured with a flow metering orifice and regulated by a butterfly valve located upstream of the orifice.

Details of the test hardware are shown in figure 2. The test hardware was mounted on a flat plate 243.84 centimeter (96.00 in.) long and 121.92cm (48.00 in.) wide. The plate was covered with two corrugated sections, figure 2(b). The corrugation had a capped leading-edge, figure 2(c). The two corrugated sections were separated by a field joint ring, figure 2(d). In the region aft of the corrugation the explosive separation strip, ("super-zip strip) was simulated-detailed in figure 2(e). A view of the vent region is shown in figure 2(f). The Titan forward skirt compartment is vented through ducts running forward of the Centaur boattail. The Tital forward skirt vent is attached to the duct and used in this test. Details of the vent-duct are shown in figures 2(g) and (h). Details of the boundary-layer thickeners are shown in figure 3.

INSTRUMENTATION

Static pressure instrumentation is shown in figure 4(a). The axial distance along the plate, X/LREF, is given in Table I. Where X is measured from tunnel station 650.75cm (256.20 in) and LREF = 2.54cm (1.00 in). The boundary-layer survey rakes are shown in figure 4(b). The boundary-layer survey hardware consisted of two rakes. The larger rake had 19 probes and was mounted under the corrugation crest. The lower five probes were concealed by the corrugation crest. The small rake had 6 probes and was located in the corrguation trough. The two rakes surveyed a 33.02cm (13.00 in) boundary layer depth. Normal distance from the corrugation trough to each probe is given in the table of figure 4(b).

The boundary layer rakes were used to survey the local flow field and to measure the boundary layer height. Rakes were located at tunnel stations 626.11cm and and 628.65cm (246.50 in. and 247.50 in.) small and large rakes, respectively. The small rake was 32.89cm (12.95 in.) above the plate centerline and the large rake was 21.21cm (8.35 in.). The field joint ring instrumentation is shown in figure 4(c). The duct and flow system instrumentation is shown in figure 4(d).

CONFIGURATIONS

A configuration summary is given in Table II. Two configurations were tested with variation in the boundary layer thickeners.

RESULTS AND DISCUSSION

At each Mach number a zero flow reading was taken with both the butterfly and gate values closed. The local static pressure to be used in the vent pressure ratio was taken as the average of the pressure upstream (orifice 202) and downstream (orifice 204) of the honeycomb vent. The vent pressure ratio, PE/P1, is defined as the ratio of the average local static pressure (at no flow condition) to plenum pressure.

The local Mach number, M_1, measures at the honeycomb vent, for zero vent flow condition is shown in figure 5. In general, the local Mach number showed only small deviations from the free stream Mach number.

The boundary-layer velocity profiles are shown in figure 6 over the Mach number range tested. A distortion occurred in the profiles between the sixth and seventh probes as a result of using the two rakes; a small rake (first six probes) in the corrugation trough and a larger rake proturding through the corrugation crest (with the seventh probe near the crest surface). The velocity profile was used to obtain the boundary-layer parameters shown in figure 7.

Two boundary-layer thickener configurations were tested to produce a variation in the boundary-layer characteristics. Configuration 1 thickeners consisted of 4 rows of 12.7 (5 in) height rods (18 per row) and was used over a Mach number range from 1.10 to 1.80. With this configuration the boundary-layer parameters are generally higher than those for configuration 2, figure 2. Configuration 2 consisted of 1 row of 12.70cm (5 in) height rods-and 1 row of 7.62cm (3 in) rods with row containing 18 rods. Configuration 2 was tested from Mach 0.80 to 1.96.

The effectiveness of the thickeners in thickening the boundary-layer is shown in figure 7(a). Configuration 1 had the thickest boundary-layer over the Mach number range where both configurations were tested. Displacement thickness for the two configurations is shown in figure 7(b). Again, configuration 1 had the largest displacement thickness. The boundary-layer shape factor is shown in figure 7(c). Also shown in this figure is the turbulent boundary-layer shape factor taken from ref. 10. The deviation of the experimental data from that of ref. 10 reflects the effects of both the field joint ring and boundary-layer thickeners.

Variation of the vent discharge coefficients with the vent pressure ratio is shown in figure 8 for the free stream Mach numbers investigated. Also presented for each configuration is the local Mach number for the zero vent flow condition. Where both sets of boundary layer thickeners were used, the vent discharge coefficient was higher with configuration 1 which produced a thicker boundary layer.

Pressure coefficient distributions for zero vent flow conditions are shown in figure 9. The pressures downstream of the field joint ring and upstream of the explosive separation strip, ("super-zip" strip) were generally less than freestream static pressure over the Mach number range tested. With the thicker boundary-layer, configuration 1, the pressure rise ahead of the field joint

ring was generally lower. However, initially, the pressure coefficient for the thicker boundary layer was higher. Downstream of the field joint ring configuration 1, with the thicker boundary layer, had smaller pressure drop.

The effect of vent flow on the pressure distributions is shown in figure 10. Generally, the effect of vent flow was to increase the pressure upstream of the vent and decrease the pressure downstream of the vent.

SUMMARY OF RESULTS

An experimental investigation was conducted in the Lewis Research Center 8-by 6-foot Supersonic Wind Tunnel to determine the discharge coefficients of the Titan forward skirt compartment vent. The test was conducted with full scale simulated flight hardware over a freestream Mach number range of 0.80 to 1.96 with the vent and corrugations mounted to a flat plate. The flat plate was flush mounted to the tunnel sidewall such that the centerlines coincided. Air was discharged from a duct through a honeycomb vent into the freestream. Vent pressure ratio was varied from about 1.00 to 0.55.

The following observations were made:

1. Generally, the vent discharge coefficient is affected by the boundary layer characteristics. For example, an increase in boundary layer neight and/or displacement thickness resulted in an increase in the vent discharge coefficient. Where both sets of boundary layer thickeners were used the vent discharge coefficient was the highest for the thicker boundary-layer conditions.

2. With no vent flow, the static pressures aft of the field joint ring (includes the vent region) were generally less than freestream static pressure over the Mach number range tested.

3. The effect of vent flow on the static pressure distribution was to increase the pressure upstream of the vent and decrease the pressure downstream of the vent.

REFERENCES

1. Johns, Albert L.; and Jones, Merle L.: Venting Characteristics of Gaseous Helium and Nitrogen Discharging into a Free Stream at Mach Numbers from 0.60 to 1.57. NASA TM X-2995, 1974.

2. Johns, Albert L.; and Jones, Merle L.: Effects of Flanges on Pressure Distribution on a Flat Plate and on an Corrugated Surface at Mach Numbers from 0.60 to 1.97. NASA TM X-2968, 1974.

3. Vick, Allen R.: An Investigation to Determine the Discharge and Thrust Characteristics of Auxiliary-Air Outlets for a Stream Mach Number of 3.25. NASA TN D-1478, 1962.

4. Kalivretenos, C. A.; Leonas, A. P.; and Franqsen, N. P.: Weight Flow Rates Through Circular Holes in a Flat Plate Immersed in a Subsonic or Supersonic Airstream. NOL-TR-61-125, United States Naval Ordinance Lab., 1963.

5. Callaghan, Edmund E.; and Bowden, Dean T.: Investigation of Flow Coefficients of Circular, Square, and Elliptical Orifices at High Pressure Ratios. NACA TN-1947, 1949.

6. Struck, H. G.; and Harkins, John A.: Compartment Venting and Pipe Flow With Heat Addition. NASA TM X-53734, 1968.

7. Walters, W. P.; Glasgow, R. W.; and Baker, J. M.: Generalized Gaseous Discharge Characteristics of Flat Plate Orifices. (TR-794-8-434, Nortronics; NASA Contract NAS8-20200.) NASA CR-98482, 1968.

8. Ramsey, P. E.: Flow Characteristics of Orifices for Venting Launch Vehicle Compartments. Research Achievements Review. Volume 3: Aerophysics Research at Marshall Space Flight Center, NASA TM X-53799, 1968, pp. 25-34.

9. Compartment Venting: Space Vehicle Design Criteria. NASA SP-8060, 1970.

10. Tucker, Maurice: Approximate Calculation of Turbulent Boundary-Layer Development in Compressible Flow, NACA TN-2337, 1951.

TABLE I. - TEST STATIC PRESSURE ORIFICES LOCATION

Region	Static pressure orifice no.	Axial distance ratio X/Lref
Upstream trough	100	-74.13
↓	101	-68.13
	102	-62.13
	103	-56.13
	104	-50.13
	105	-44.13
	106	-40.13
	107	-37.13
	108	-35.13
	109	-33.73
Field joint ring	300	-33.38
Field joint ring	301	-32.98
Field joint ring	302	-32.78
Upstream trough	110	-31.88
↓	111	-31.48
	112	-30.48
	113	-28.48
	114	-24.48
	115	-20.48
	116	-18.48
	117	-17.48
	118	-16.48
Upstream crest	200	-17.48
Upstream crest	201	-16.48
Upstream crest	202	-15.58
Below vent 21.40 cm (8.41 in.)	203	-9.70
Below vent 7.11 cm (2.80 in.)	208	-9.70
Below vent 11.88 cm (4.67 in.)	209	-9.70
Downstream trough	119	-8.08
Downstream trough	120	-7.08
Downstream trough	121	-5.58
Downstream crest	204	-8.58
↓	205	-7.58
	206	-6.58
	207	-5.08
Super-zip	303	-3.51
Super-zip	304	-2.51

TABLE II. - CONFIGURATION SUMMARY

Configuration		Boundary - layer thickener
Symbol	Number	
O	1	4 rows 12.70 cm (5 in.) height rods (18 per row)
◊	2	1 row 12.70 cm (5 in.) height rods 1 row 7.62 cm (3 in.) height rods (18 per row)

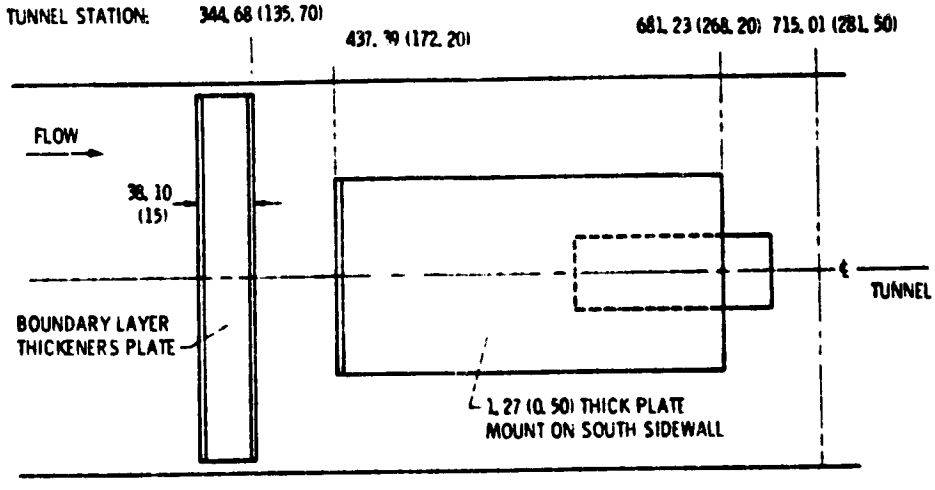

(a) Schematic of test installation.

Figure 1. - Test installation in 8- by 6-foot supersonic wind tunnel. (All dimensions are in cm (in.).)

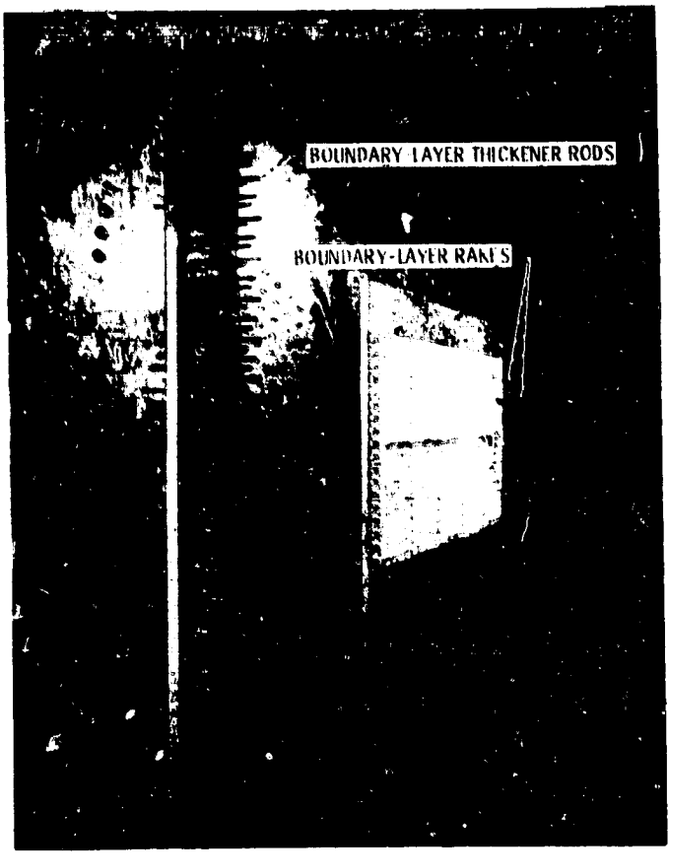

(b) Test installation with 4 rows of 12.70 cm (5 in.) boundary-layer thickener rods.

Figure 1. - Continued.

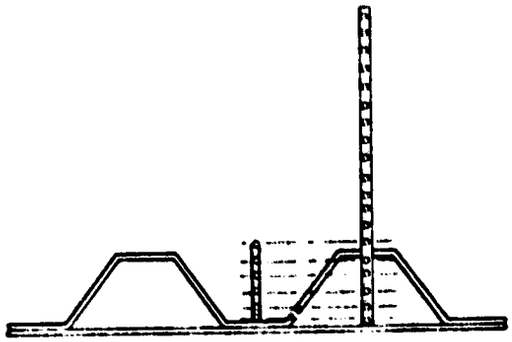

(c) Boundary - layer survey rakes.

Figure 1. - Continued

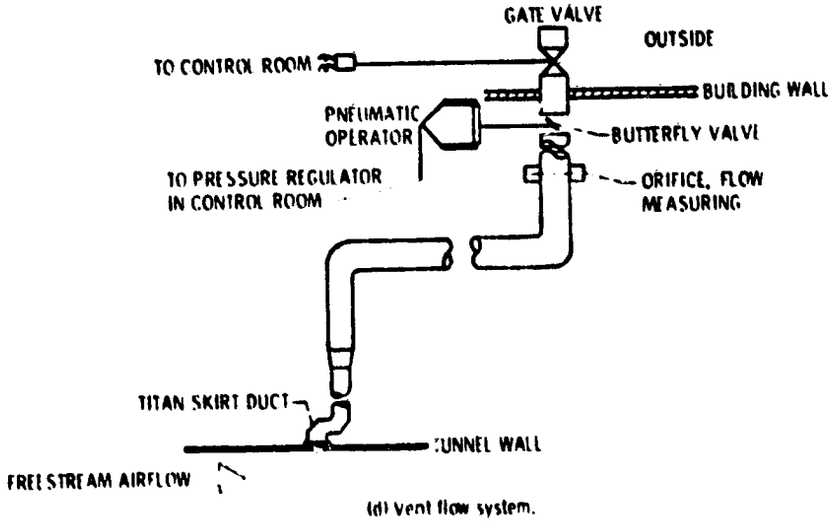

(d) Vent flow system.

Figure 1. - Concluded

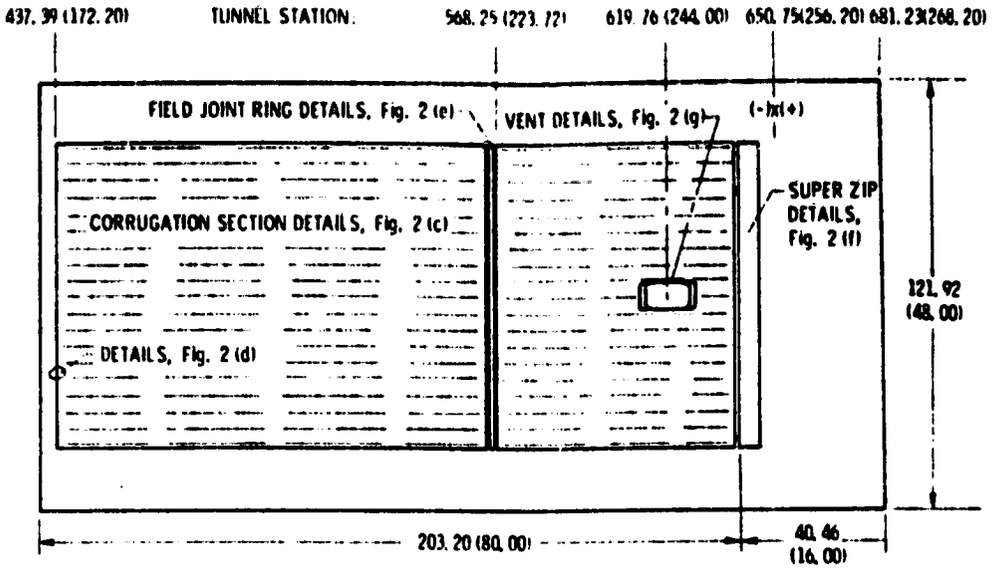

(a) Assembly of test.

Figure 2. - Details of test geometry. Dimensions are in centimeters (in.).

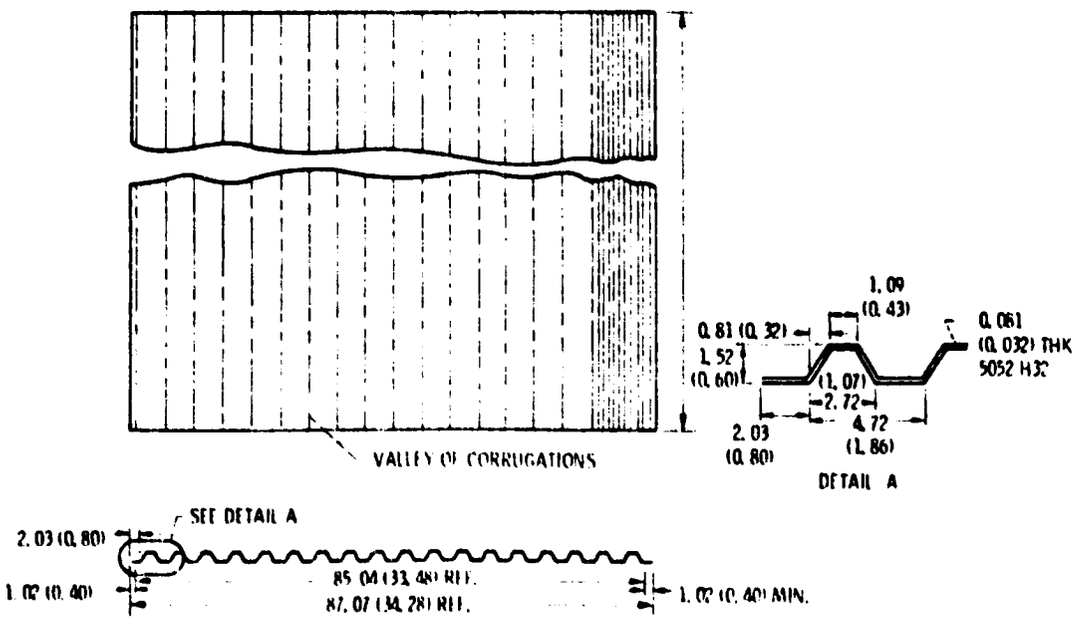

(b) Corrugated panels and cross section details.

Figure 2. Continued.

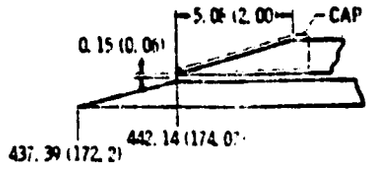

(c) Leading-edge of corrugation details.

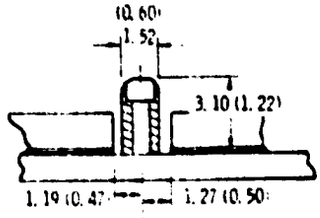

(d) Field joint ring details.

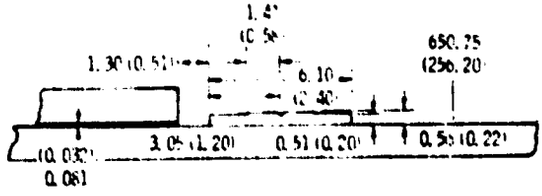

(e) Super-zip region details.

Figure 2. - Continued.

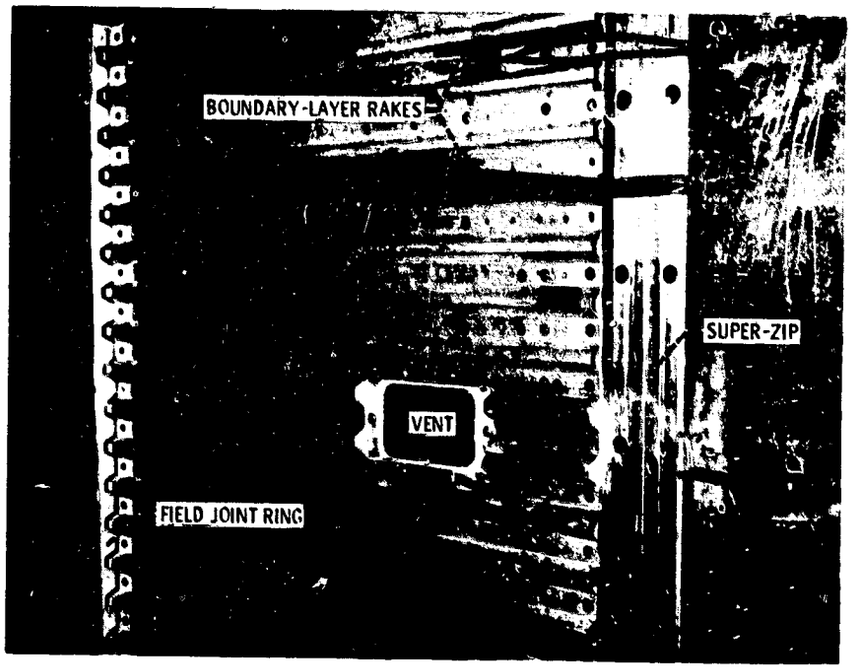

(f) View of vent region.

Figure 2. - Continued.

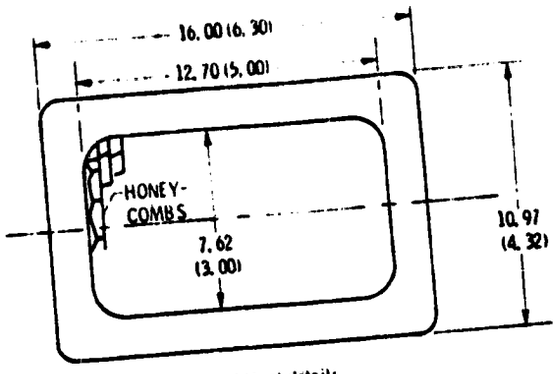

(g) Vent details.

Figure 2. - Continued.

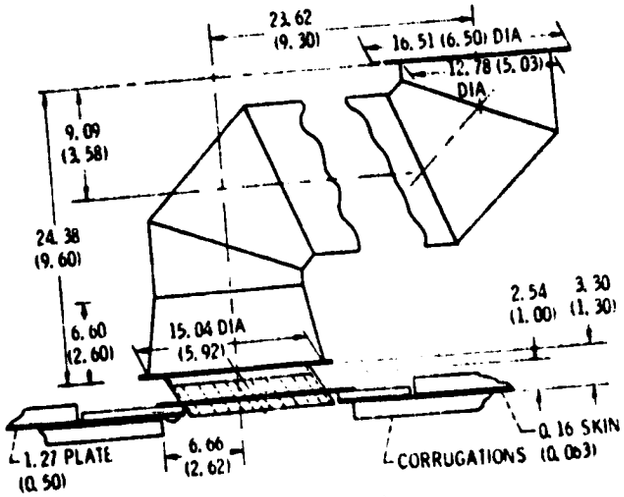

(h) Details of duct.

Figure 2. - Concluded.

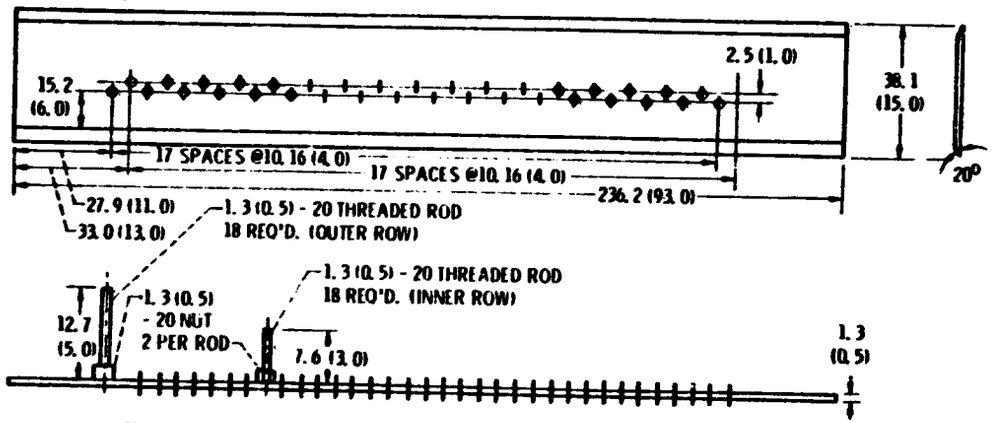

Figure 3. - Details of boundary-layer thickeners. Dimensions are in centimeters (in.).

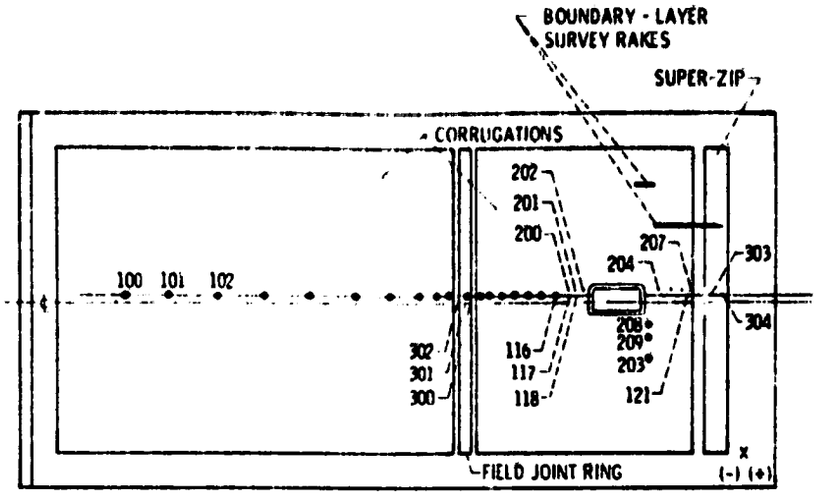

(a) Test instrumentation.

Figure 4. - Instrumentation.

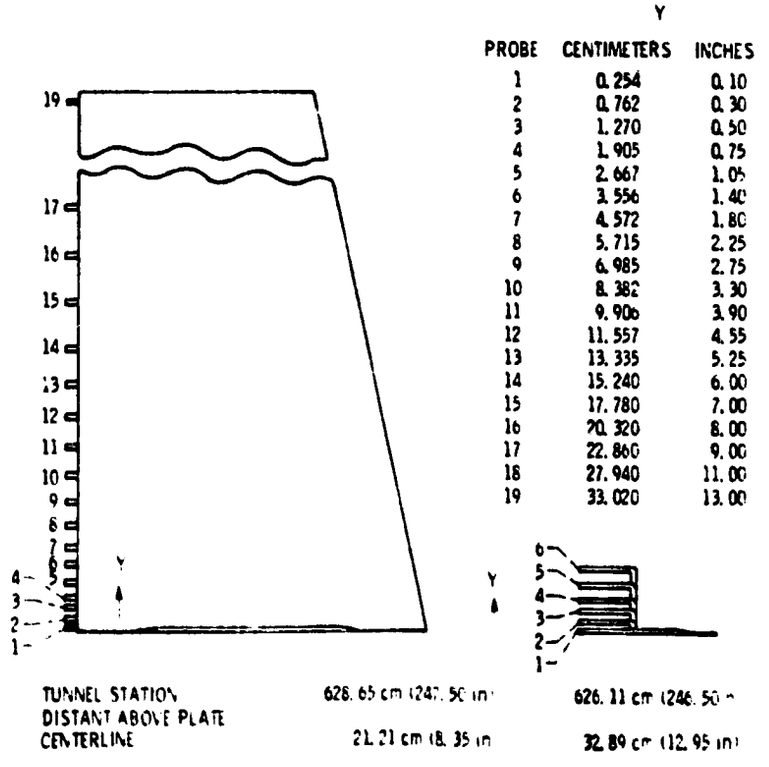

(b) Boundary-layer survey rakes.

Figure 4. - Continued.

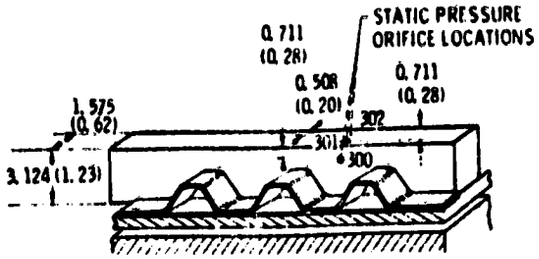

(c) Field joint ring instrumentation.

Figure 4. - Continued.

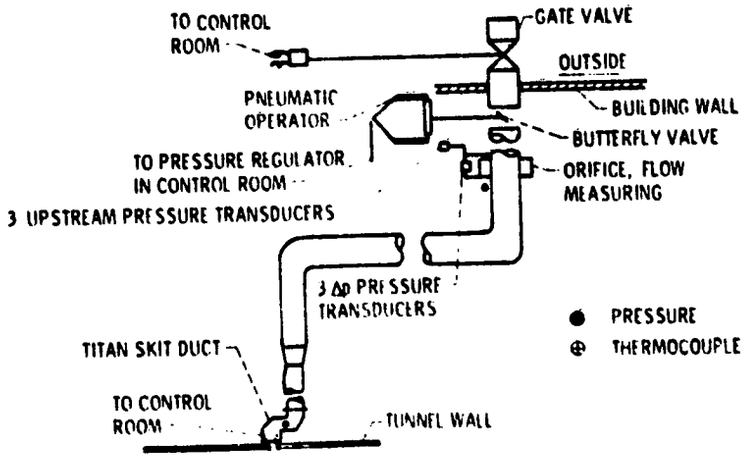

(d) Duct and flow system instrumentation.

Figure 4. - Concluded.

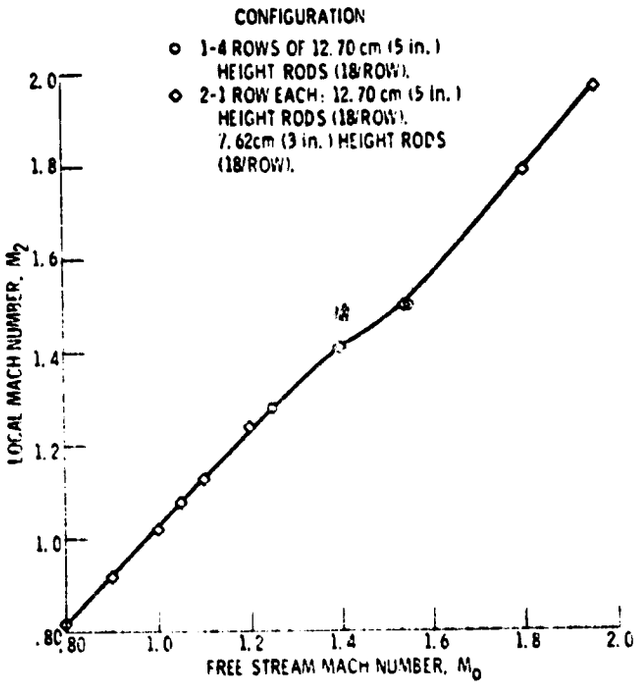

Figure 5. - Variation of local Mach number with free stream Mach number.

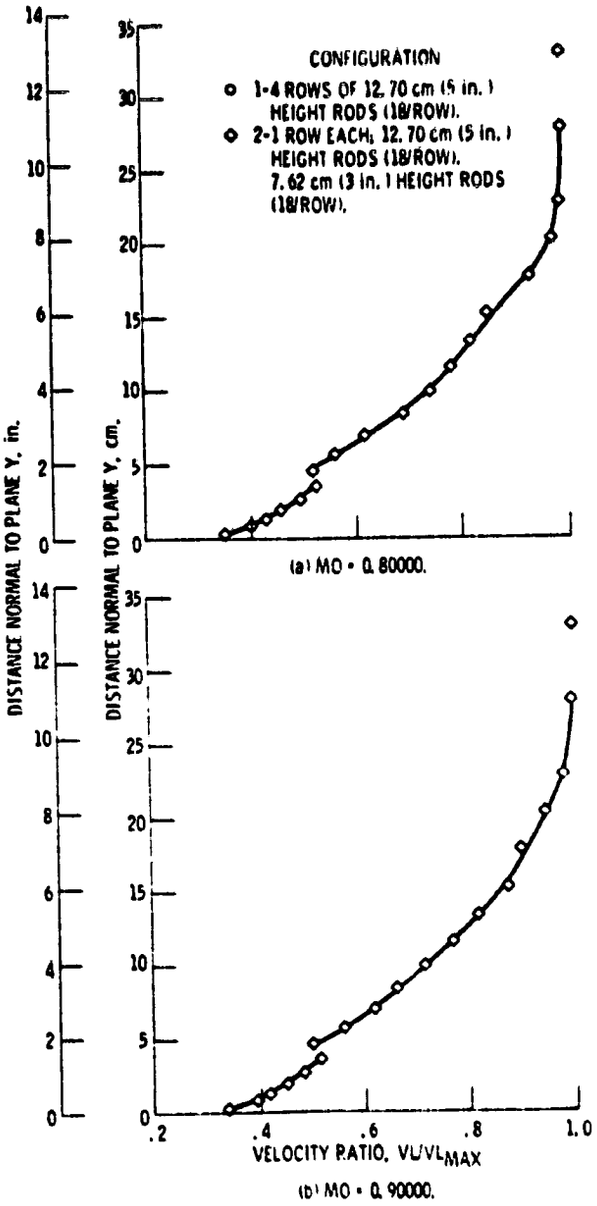

Figure 6. - Boundary-layer velocity profiles.

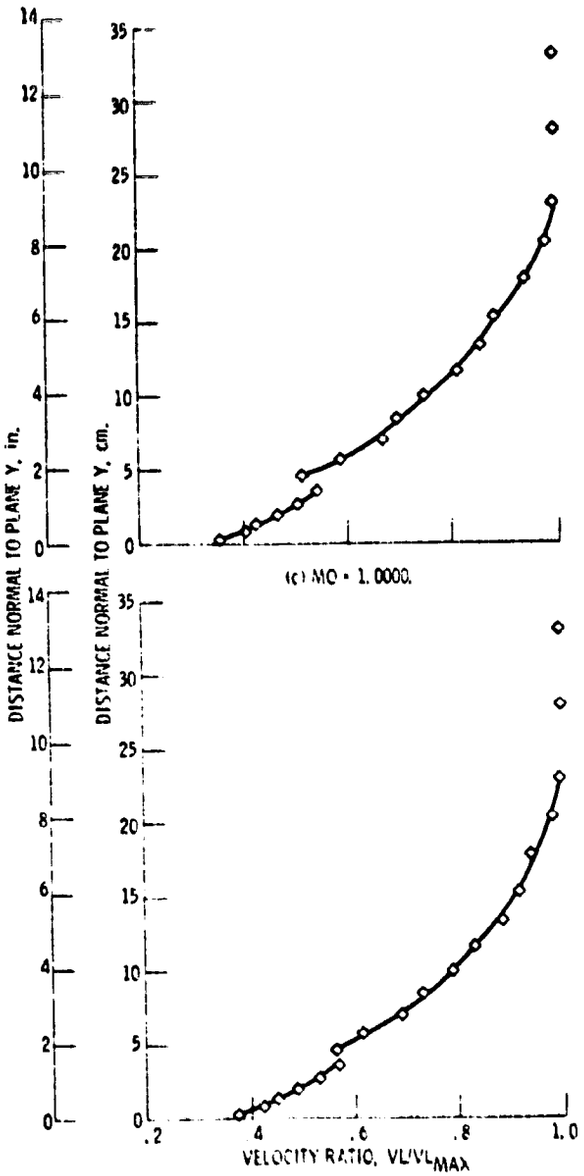

(c) MO = 1.0000.

(d) MO = 1.0500.

Figure 6. - Continued.

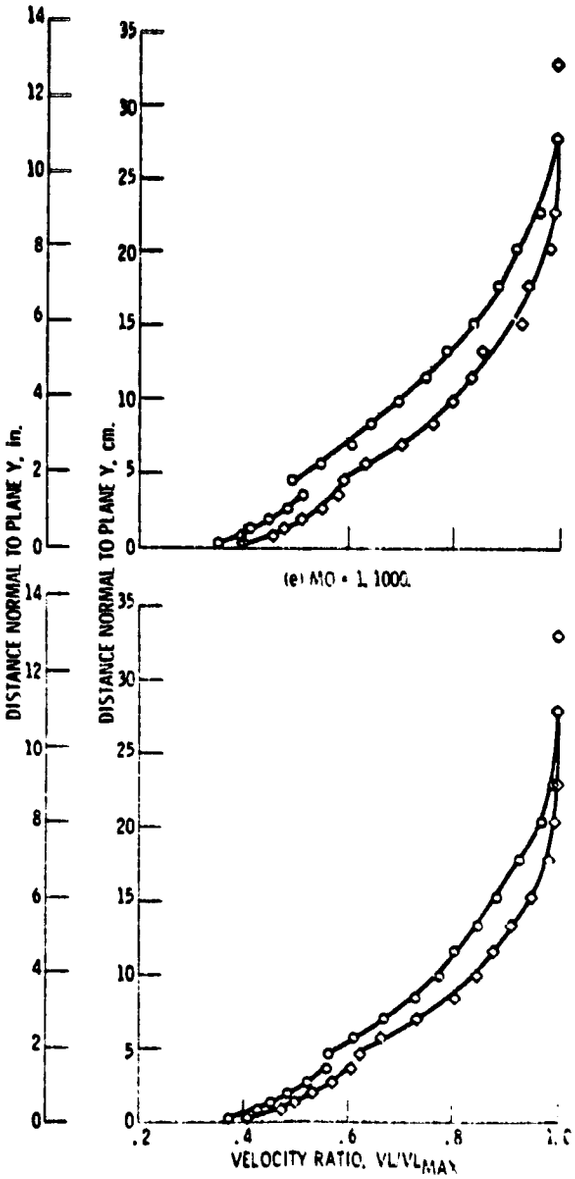

Figure 6. - Continued.

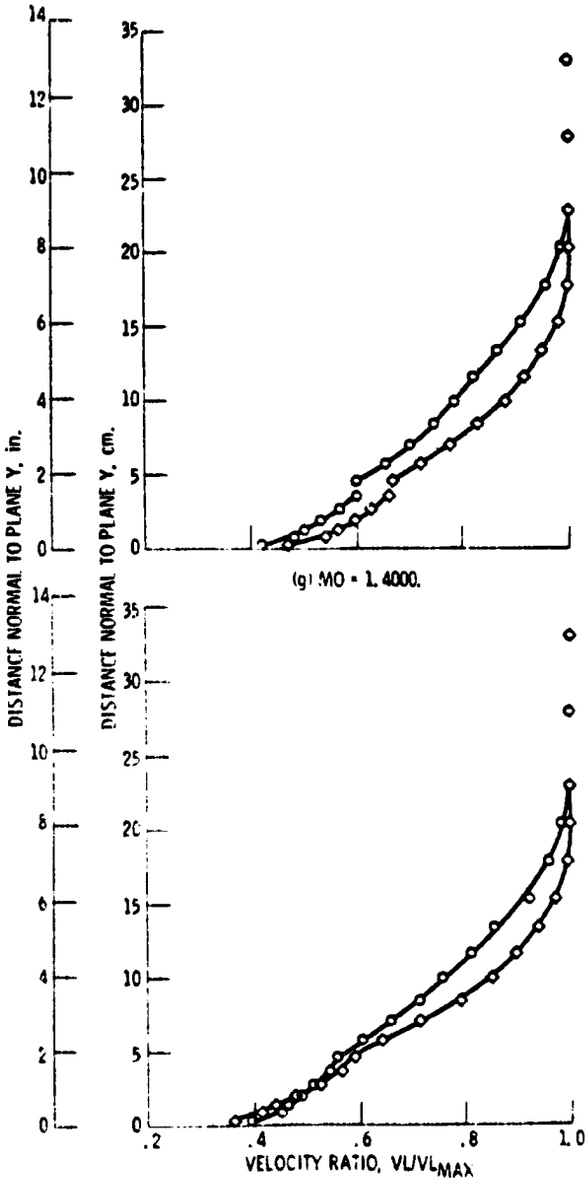

(g) MO = 1.4000.

(h) MO = 1.5500.

Figure 6. - Continued.

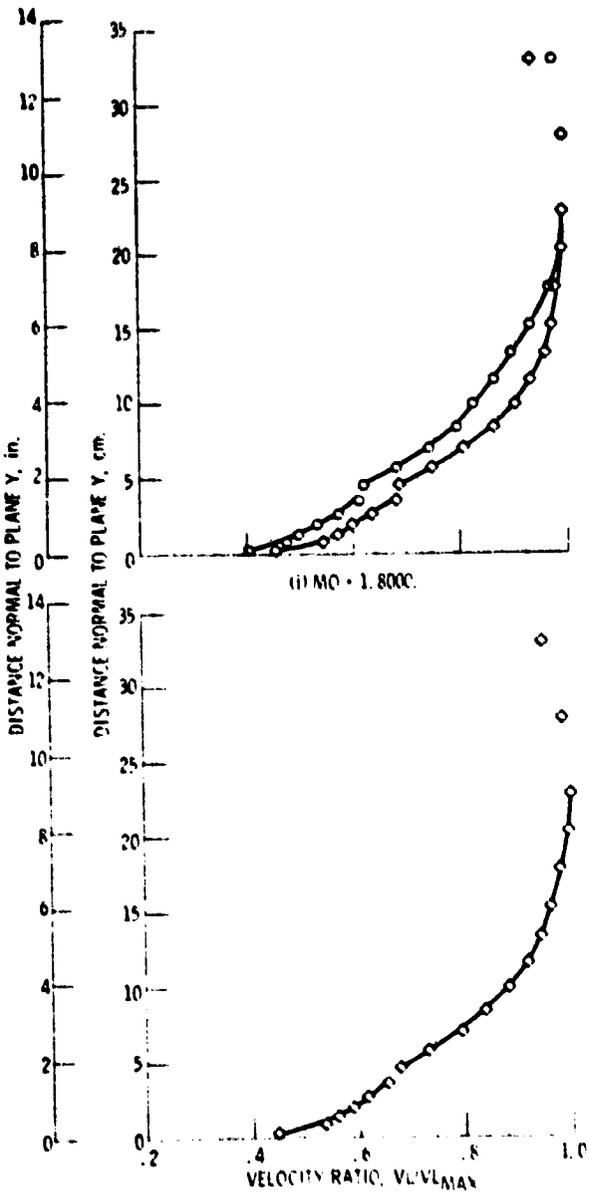

(i) MO = 1.8000.

(j) MO = 1.9600.

Figure 6. - Concluded.

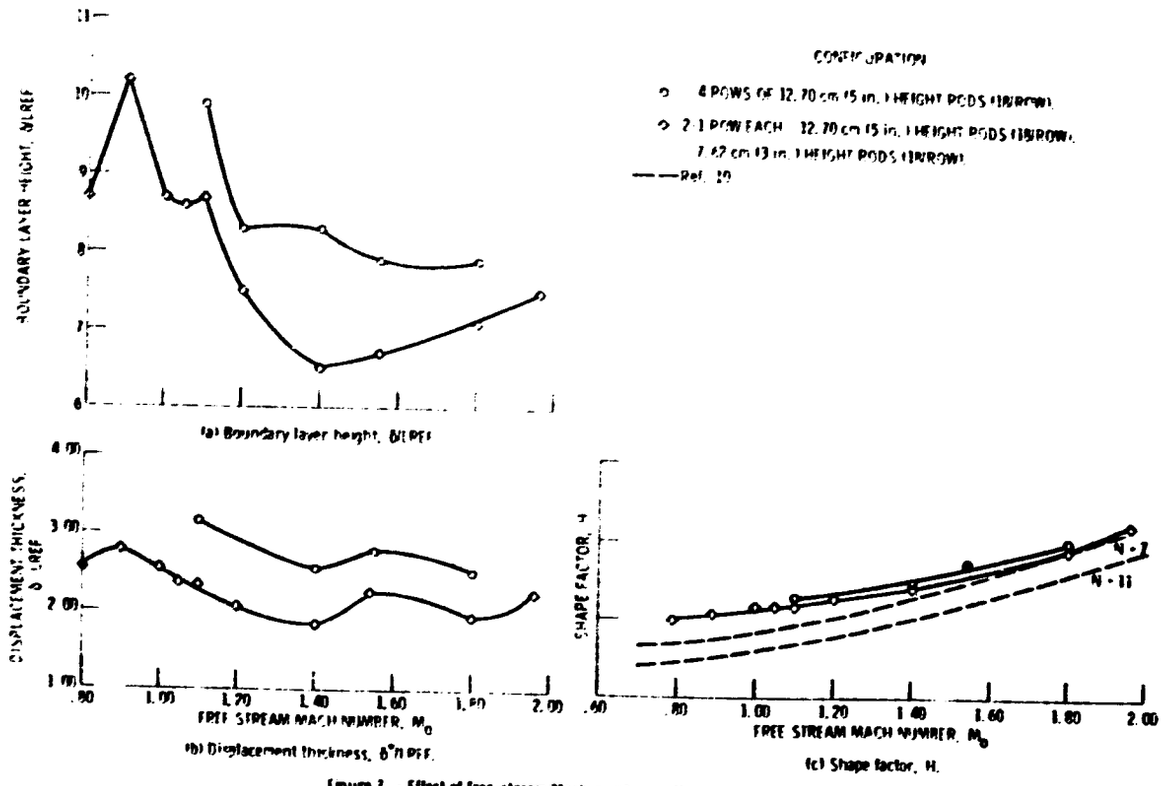

(a) Boundary layer height, δ/REF

(b) Displacement thickness, δ*/REF

(c) Shape factor, H

Figure 7 - Effect of free-stream Mach number on the boundary layer parameters.

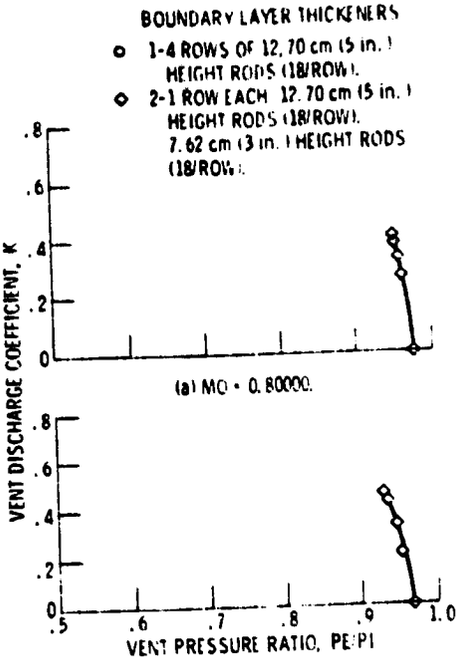

(a) MO = 0.80000.

(b) MO = 0.90000.

Figure 8. - Variation of vent discharge coefficient with vent pressure ratio.

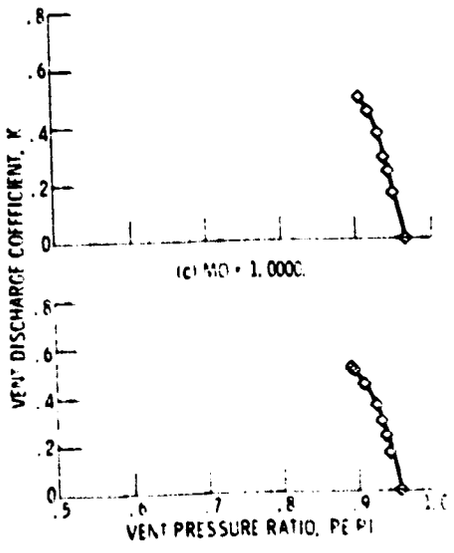

(c) MO = 1.0000.

(d) MO = 1.0500.

Figure 8. - Continued.

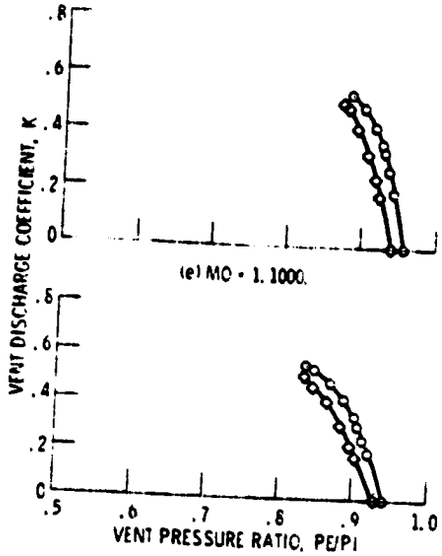

(e) MO = 1.1000.

(f) MO = 1.2000.

Figure 8. - Continued.

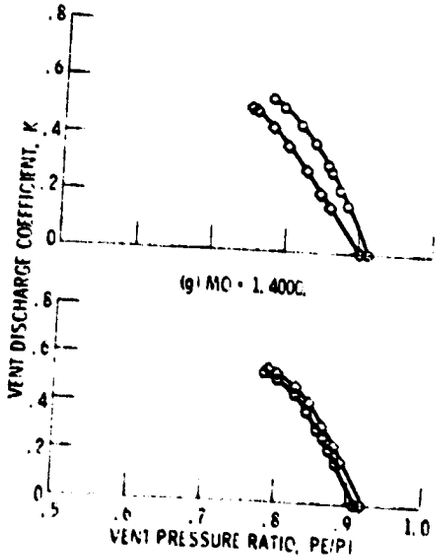

(g) MO = 1.4000.

(h) MO = 1.5500.

Figure 8. - Continued.

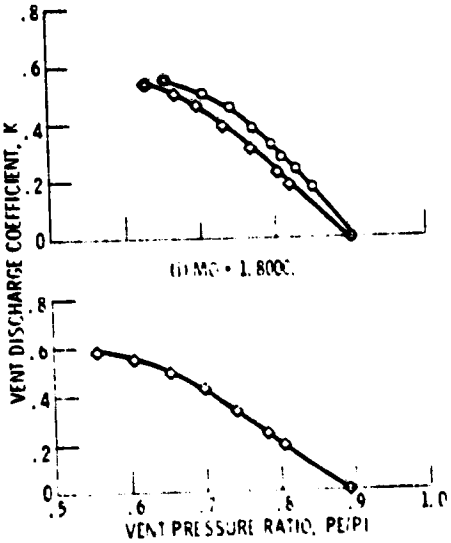

(f) M_G = 1.800.

(g) M_G = 1.900

Figure 8. - Concluded.

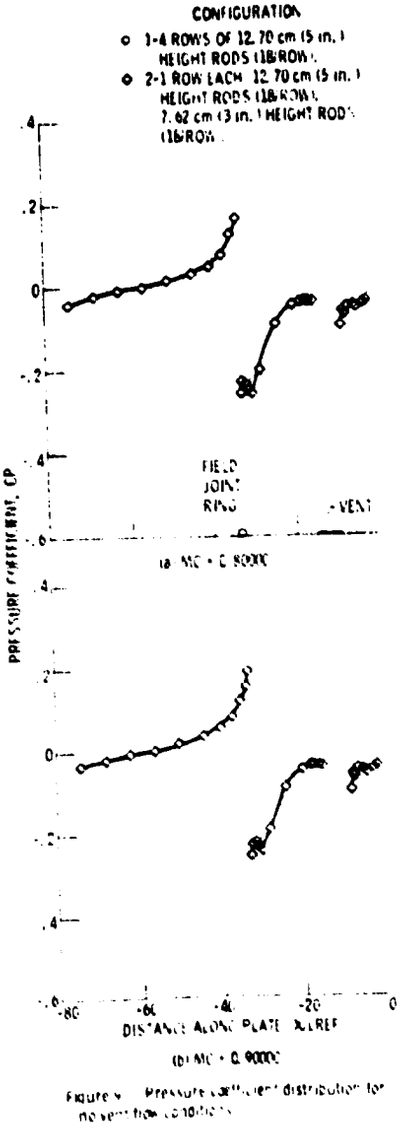

Figure 9. Pressure coefficient distribution for no vent flow conditions.

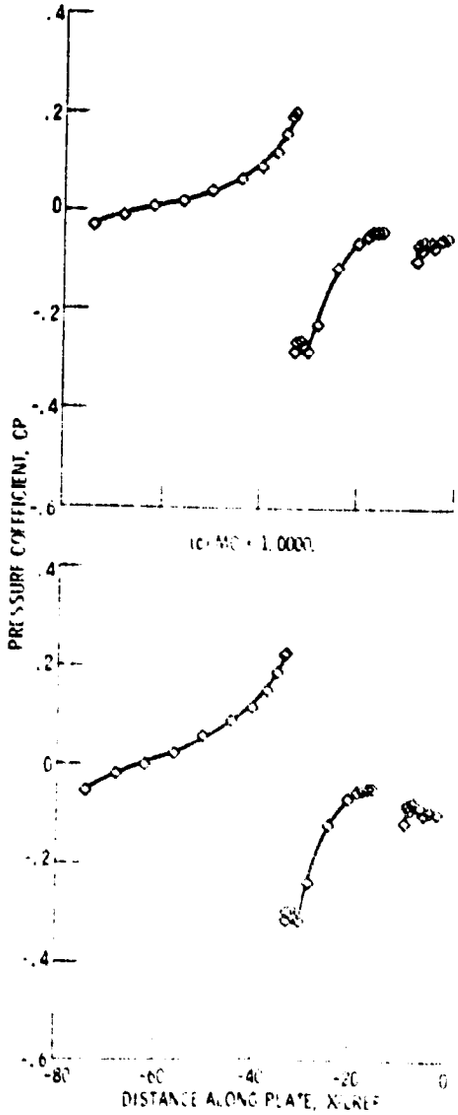

Figure 9 - Continued

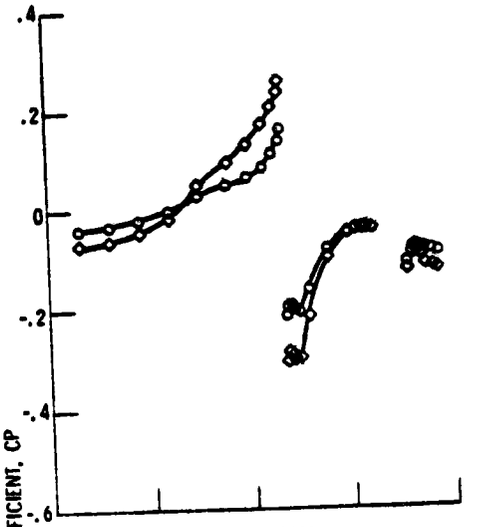

(e) MO = 1.1000.

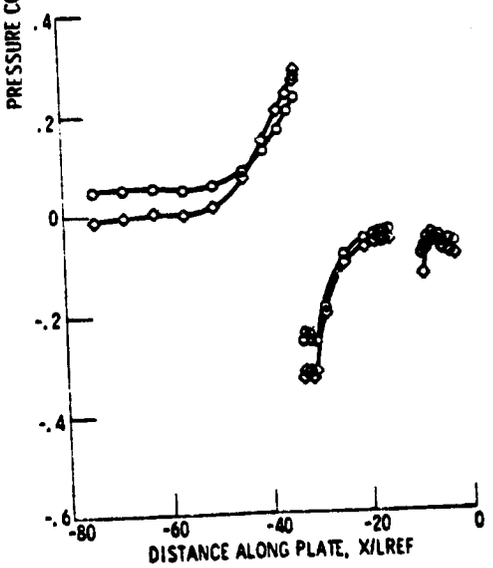

(f) MO = 1.2000.

Figure 9. - Continued.

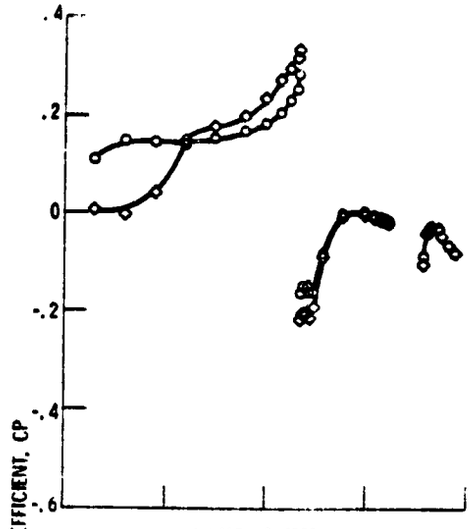

(g) MO = 1.4000.

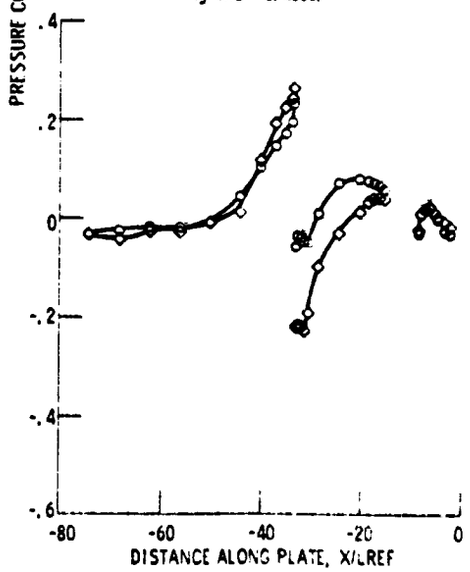

(h) MO = 1.5500.

Figure 9. - Continued.

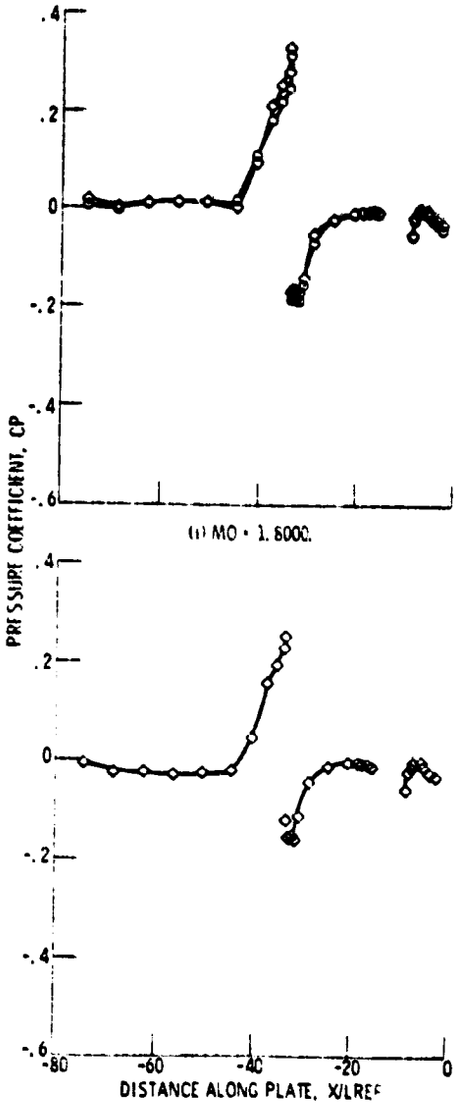

Figure 9. - Concluded.

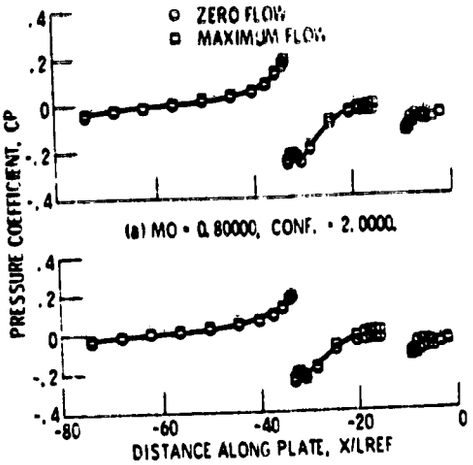

(a) MO = 0.80000, CONF. = 2.0000.

(b) MO = 0.90000, CONF. = 2.0000.

Figure 10. - Effect of vent flow on the pressure distributions.

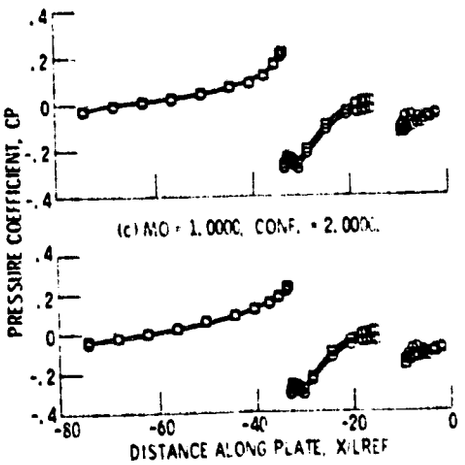

(c) MO = 1.0000, CONF. = 2.0000.

(d. MO = 1.0500, CONF. = 2.0000.

Figure 10. - Continued.

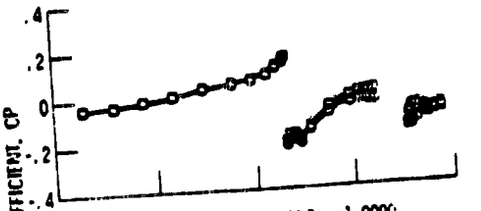

(e-1) MO = 1.1000, CONF. = 1.0000.

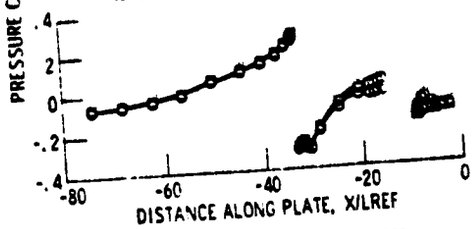

(e-2) MO = 1.1000, CONF. = 2.0000.

Figure 10. - Continued.

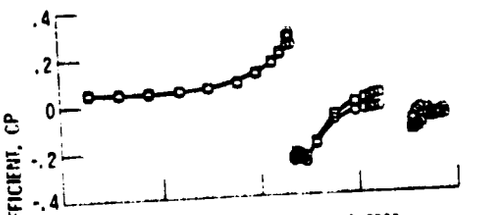

(f-1) MO = 1.2000, CONF. = 1.0000.

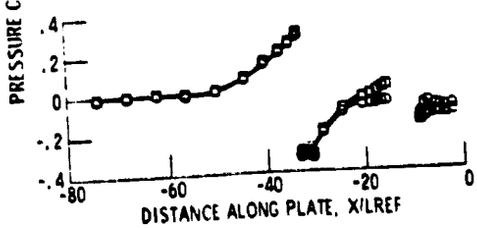

(f-2) MO = 1.2000, CONF. = 2.0000.

Figure 10. - Continued.

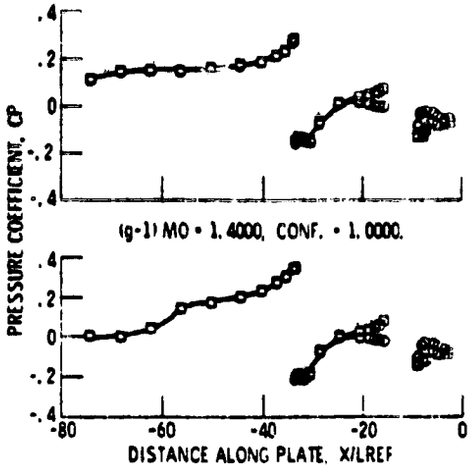

(g-1) MO = 1.4000, CONF. = 1.0000.

(g-2) MO = 1.4000, CONF. = 2.0000.

Figure 10. - Continued.

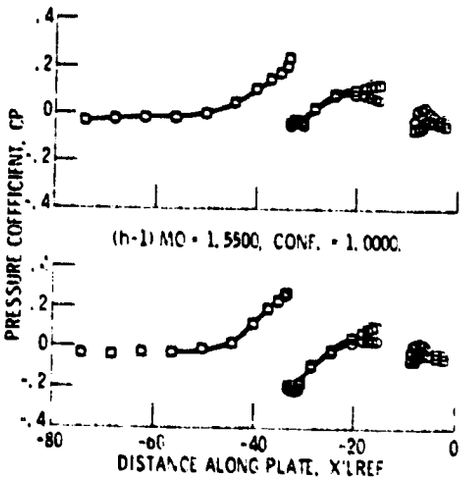

(h-1) MO = 1.5500, CONF. = 1.0000.

(h-2) MO = 1.5500, CONF. = 2.0000.

Figure 10. - Continued.

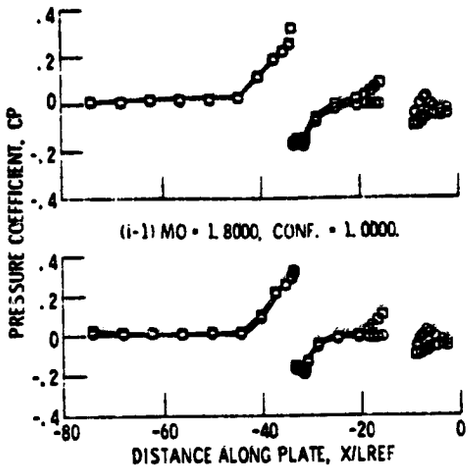

(i-1) MO = 1.8000, CONF. = 1.0000.

(i-2) MO = 1.8000, CONF. = 2.0000.

Figure 10. - Continued.

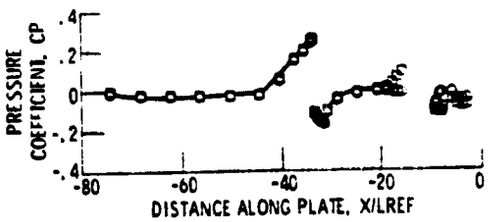

(j) MO = 1.9600, CONF. = 2.0000.

Figure 10. - Concluded.